Dalton Transactions

PAPER

View Article Online
View Journal | View Issue

Cite this: *Dalton Trans.*, 2015, **44**, 9140

A facile ultrasonication assisted method for Fe_3O_4@SiO_2-Ag nanospheres with excellent antibacterial activity

Shuang-Sheng Chen,†[a] Hui Xu,†[a] Hua-Jian Xu,[b] Guang-Jin Yu,*[a] Xing-Long Gong,[c] Qun-Ling Fang,*[b] Ken Cham-Fai Leung,[d] Shou-Hu Xuan[c] and Qi-Ru Xiong*[a]

Received 11th March 2015,
Accepted 30th March 2015

DOI: 10.1039/c5dt00977d

www.rsc.org/dalton

To increase the monodispersity of magnetic hybrid nanocomposites, a novel ultrasonic method was introduced to synthesize uniform Fe_3O_4@SiO_2-Ag nanospheres. The immobilized Ag nanocrystals were tunable by varying the experimental conditions. An antibacterial assay indicated that the Fe_3O_4@SiO_2-Ag nanospheres exhibited excellent antibacterial activities against *Staphylococcus aureus* and *Escherichia coli*, in which the minimum inhibition concentrations (MIC) were 40 μg mL^{-1} and 20 μg mL^{-1}, respectively. The live/dead bacterial cell fluorescence stain assay agreed well with the antibacterial assay. The CCK-8 results indicated these nanospheres were bio-compatible for human normal cells and presented relative cytotoxicity against HepG2 tumor cells. These nanospheres could be easily uptaken by the cells and they could affect bacterial cells both inside and outside the cell membrane, which enable them to be promisingly applied in future biomedical areas.

1. Introduction

Pathogenic bacteria greatly threaten public health as they bring about terrible infectious diseases. To meet with the increasing demands for hygiene in public health care, various researchers have attempted to develop highly effective antibacterial agents.[1–4] In recent years, with the rapid development of nanotechnology, more and more research in this area has been focused on nano-antibacterials.[5–8] Silver has been used as an antibacterial agent for centuries to deal with infections, burns and chronic wounds due to its low toxicity toward the human body.[9–14] It was found that by decreasing the size of the Ag particles, the antibacterial activity was intensively enhanced. Therefore, the investigation of an Ag-based nano-antibacterial agent would be more helpful for its future commercial production and application in clothing, food packaging and bandages.[15,16]

Though the principle was not very clear, the most acceptable antibacterial mechanism of Ag nanoparticles was believed to be the release of Ag ions, which can combine –SH groups and lead to inactivation of proteins.[17–19] Besides the size and shape, the stability of the nanoparticles also exhibited a high influence on antibacterial activity.[10,20] Therefore, Ag nanoparticles have been immobilized onto various substrates such as silica, polymers, iron oxide, carbon, layered double hydroxide (LDH), zeolite, *etc.*[21–30] This method not only prevented the aggregation of Ag nanoparticles but also enhanced their antibacterial capacity. Present research demonstrated that Ag-based nano-antibacterial agents could affect the bacteria both inside and outside the cell membrane by catalyzing the complete destructive oxidation of the microorganism.[18,31] To this end, uniform Ag-based nanocomposites with small sizes are desirable for high performance nano-antibacterial agents.

Environmentally friendly methods are favorable for the preparation of nano-antibacterial agents since they can reduce the biological hazard for living cells.[18,32–36] Recently, several *in situ* fabrication strategies have been developed to eliminate the residue of the toxic reducing agents (such as KBH_4 and hydrazine) in the final system. By utilizing the reducing characteristics of polydopamine (PDA), Ag nanoparticles with different sizes and coverage were coated onto the surface of PS/PDA microspheres and the thereof antibacterial agent exhibited enhanced performance against *Escherichia coli* and *Staphylococcus aureus*.[37] Similarly, the Ag nanoparticles could be directly immobilized on the LDH film by simply immersing

[a]*Department of Chirurgery, Affiliated Hospital 1, Anhui Medical University, Hefei 230032, P.R. China. E-mail: yugj7806290@sohu.com, xiongqiru2012@126.com*
[b]*School of Medical Engineering, Hefei University of Technology, Hefei 230009, P.R. China. E-mail: fql.good@hfut.edu.cn*
[c]*CAS Key Laboratory of Mechanical Behavior and Design of Materials, Department of Modern Mechanics, University of Science and Technology of China, Hefei 230026, P. R. China*
[d]*Department of Chemistry and Partner State Key Laboratory of Environment and Biological Analysis, Hong Kong Baptist University, Kowloon, Hong Kong SAR, P. R. China*
†These authors contributed equally to this work.

the film into the $AgNO_3$ aqueous solution due to a self-redox reaction.[28] This method offered a good opportunity for their practical application in antimicrobial surfaces.

Moreover, some risks of using Ag based nano-antibacterial agents were also presented because the high concentration of residual nanosilver in solution was toxic. The potential strategy for solving this problem would be the combination of magnetic characteristics with antibacterial properties, so that the antibacterial agent could target a certain area or be magnetically separated from the working area after the bacteria have been killed. During the past decade, several magnetic antibacterial agents such as Ag@Fe_3O_4 core shell nanoparticles/nanospheres, Fe_3O_4@SiO_2@Ag sub-microspheres/janus nanorods, and Ag-Fe_2O_3 heteromers have been developed.[23,38–42] Although these materials exhibited high antibacterial performance, the detailed nanostructure dependence on antibacterial activity was unknown and the mechanism of their action was not very clear. In consideration of the green preparation and easy conduction, a novel method for the synthesis of a multifunctional antibacterial agent is still needed.

In this work, a facile ultrasonication assisted method was reported for the easy and environmentally friendly synthesis of Fe_3O_4@SiO_2-Ag nanospheres. This method presented three unique characteristics: (1) different from the previously reported large Fe_3O_4@SiO_2-Ag particles, the average size of the obtained product was about 200 nm. They were uniform and could be well dispersed within PBS to form a stable suspension. (2) The small Ag nanoparticles were synthesized under sonication and neither reductant nor toxic reagents were used in this procedure. Moreover, the size of the Ag nanoparticles could be controlled by varying the reaction time. (3) The as-prepared nanoparticles could be used as an antibacterial agent against *Escherichia coli* and *Staphylococcus aureus*. Due to the small size, these materials also could be uptaken by cells which would be more helpful for further investigating their antibacterial mechanisms.

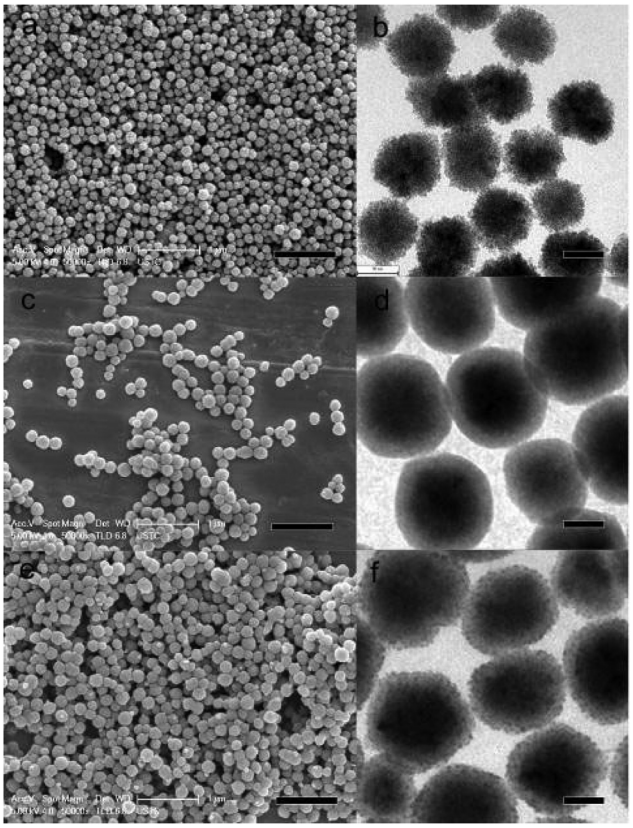

Fig. 1 SEM and TEM images of the as prepared Fe_3O_4 (a and b), Fe_3O_4@SiO_2-NH_2 (c and d), and Fe_3O_4@SiO_2-Ag nanospheres (e and f). The scale bars for the SEM and TEM images are 1 μm and 90 nm, respectively.

2. Results and discussion

2.1 Preparation and characterization of Fe_3O_4@SiO_2-Ag nanospheres

The Fe_3O_4 nanospheres were prepared according to the previously reported solvothermal method.[43] SEM images confirmed that the as-obtained product was uniform with an average diameter of 150 nm (Fig. 1). The Fe_3O_4 nanospheres presented a cluster-like nanostructure and were composed of Fe_3O_4 nanocrystals. The TEM image of the Fe_3O_4 nanosphere (Fig. 1b) clearly approved the above description and the measured size agreed well with the SEM analysis. These Fe_3O_4 nanospheres possessed a rough surface, in which the polyacrylic acid polymer was entangled to give a large amount of hydrophilic functional groups. Therefore, they can be well suspended within a water or ethanol solution.

Ultrasonication was applied to synthesize monodispersed Fe_3O_4@SiO_2-NH_2 nanospheres. Firstly, the SiO_2 layer was uniformly coated onto the surface of the Fe_3O_4 nanospheres to form a well defined core–shell nanostructure. Due to the preparation being conducted under sonication, the as-formed Fe_3O_4@SiO_2 nanospheres were monodispersed without large aggregation. At the end of the coating process, APTES was introduced into the synthetic system, thus the surface of the Fe_3O_4@SiO_2 nanospheres was *in situ* modified by a layer of $-NH_2$ groups. Ultrasonication is critical to this method as many large aggregates were formed in the product while only magnetic or mechanical stirring was conducted. The SEM image shown in Fig. 1c demonstrates the good dispersity of the nanospheres synthesized under sonication. Because of the uniform coating, the average size of the Fe_3O_4@SiO_2-NH_2 was larger than the pristine Fe_3O_4 nanospheres. The TEM image shown in Fig. 1b further proves the formation of a core–shell nanostructure. By analyzing 100 particles, the average shell thickness of the SiO_2 layer was about 30 nm. Here, the average shell thickness could be controlled by varying the experimental parameters, such as the concentration of the Fe_3O_4 nanospheres and TEOS.

The preparation of the Fe_3O_4@SiO_2-Ag nanospheres was also conducted under ultrasonication by using Fe_3O_4@SiO_2-NH_2 as the template. In this process, the $-NH_2$ group served as a bridge between the SiO_2 coating and Ag nanoparticles.

Without these functional groups, only a few Ag nanoparticles were decorated on the Fe_3O_4@SiO_2 nanospheres. After the $[Ag(NH_3)_2]^+$ ions were introduced into the Fe_3O_4@SiO_2-NH_2 suspension, they would be slowly reduced by the $-NH_2$ group and ethanol solvent to give Ag particles. Fig. 1e shows the SEM image of the Fe_3O_4@SiO_2-Ag nanospheres which clearly indicates that the as-prepared product presented monodispersibility without large aggregation. The average size of the product was similar to that of the Fe_3O_4@SiO_2-NH_2 nanospheres. However, from the TEM image (Fig. 1f), it was found that the surface of the Fe_3O_4@SiO_2-Ag nanospheres was much rougher than the Fe_3O_4@SiO_2-NH_2. All the surfaces of the nanospheres were decorated with small dots with a size of about 3–5 nm and the coverage ratio was very high. Here, sonication was important for such a high loading. During the preparation, the sonication accelerated the reducing process since "hot points" with high pressure, temperature, and reductive circumstance were formed in the solution.[44,45] Therefore, the Ag nanoparticles can directly cover the surface of the template with a high coverage ratio using this method.

Here, the sonication time had a high influence on the Ag coverage of the Fe_3O_4@SiO_2 nanospheres. Fig. 2a presents the TEM image of the Fe_3O_4@SiO_2-Ag nanospheres after 1 h of sonication. Although the Ag nanoparticles were successfully immobilized on the Fe_3O_4@SiO_2 nanospheres, the coverage in this case was not very high. As soon as the sonication time was prolonged to 3 h, the uniform coating of a Ag layer was obtained. A further increase of the reaction time is not good for the preparation of the Fe_3O_4@SiO_2-Ag nanospheres. It was found that the size of the Ag nanoparticles critically increased from 3–5 nm to 10–20 nm. Moreover, some Ag–Ag nanoparticle aggregates were found on the nanospheres' surface. Therefore, 3 h is the optimum time for this preparation. The typical high magnification TEM image of a single Fe_3O_4@SiO_2-Ag nanosphere (Fig. 2d) indicates that the Ag nanodots were homogeneously distributed on the surface. These Ag nanodots were tightly anchored on the Fe_3O_4@SiO_2 core with the help of abundant amine groups. The EDS (energy-dispersive X-ray spectroscopy) results in Fig. 2e also indicate that this nanosphere was composed of the elements Fe, Si, O, and Ag, which further hinted at successful preparation.

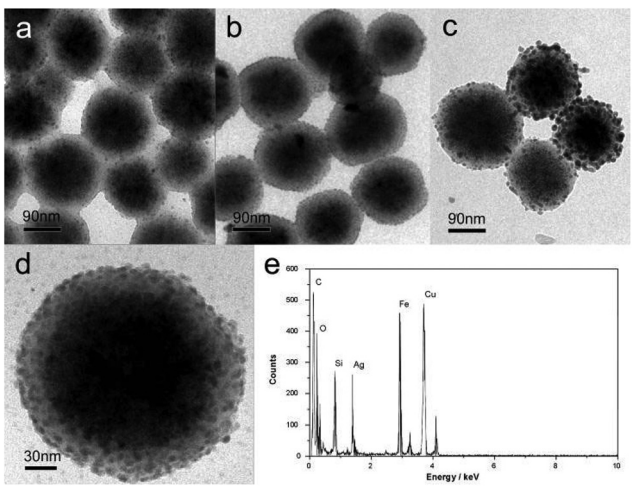

Fig. 2 TEM images of the Fe_3O_4@SiO_2-Ag nanospheres prepared under different ultrasonication times: (a) 1 h; (b) 3 h; (c) 10 h. (d) and (e) are the large magnification TEM image and EDS spectra for the nanospheres prepared under 3 h, respectively.

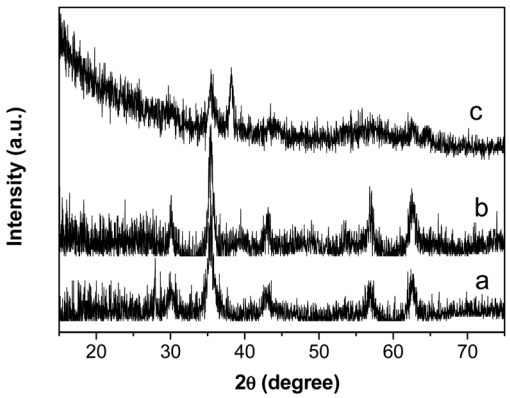

Fig. 3 XRD diffraction patterns of the as-prepared Fe_3O_4 (a), Fe_3O_4@SiO_2-NH_2 (b), and Fe_3O_4@SiO_2-Ag (c) nanospheres.

The XRD spectra of the as-prepared samples at different steps are shown in Fig. 3, including the Fe_3O_4, Fe_3O_4@SiO_2-NH_2, and Fe_3O_4@SiO_2-Ag nanospheres. The broad nature of the diffraction peaks for Fe_3O_4 illustrates the cluster-like nanostructure. Because of the amorphous crystallinity of the SiO_2 shell, a novel obvious peak for the SiO_2 has not been observed in the Fe_3O_4@SiO_2-NH_2 product. The further immobilization of Ag nanoparticles on the Fe_3O_4 nanospheres lead to the presence of a novel broad diffraction peak located at 38°. According to the Scherrer formula, the average size of the Ag nanoparticles was calculated to be 5 nm.[46] This result also agreed well with the above TEM and SEM analysis. XPS was also used to analyze the surface state of the materials. As shown in Fig. 4a, C1s, O1s, Si2p and N1s signal peaks are distinct in the XPS spectra, which demonstrates that the Fe_3O_4 nanospheres were well encapsulated by the SiO_2 shell. The relative weak peak for N1s indicated that the SiO_2 shell was functionalized by an amine group. After the Ag nanoparticles were decorated on the Fe_3O_4@SiO_2 nanospheres, strong peaks at a binding energy of about 368 and 374 eV were present which demonstrated that metallic Ag with a zero covalent state was formed in the nanospheres.[37]

2.2 Antibacterial properties of Fe_3O_4@SiO_2-Ag nanospheres

Because of its low toxicity to humans, both silver and silver-based nanomaterials have been extensively used as antimicrobial agents due to their strong inhibitory effects for a wide range of bacteria.[10,47] In this work, both *Escherichia coli* and *Staphylococcus aureus* were applied as bacterium models to study the antibacterial properties of the Fe_3O_4@SiO_2-Ag nanospheres.

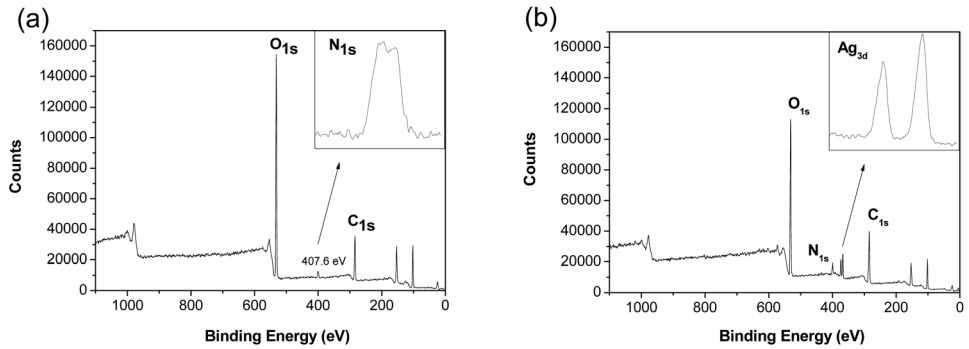

Fig. 4 XPS spectra of the as-prepared Fe_3O_4@SiO_2-NH_2 (a) and Fe_3O_4@SiO_2-Ag nanospheres (b); the insert for (a) and (b) are the N1s and Ag3d spectra, respectively.

Here, a modified Kirby-Bauer method was used to quantitatively investigate the antibacterial activities of the Fe_3O_4@SiO_2-Ag nanospheres. The Fe_3O_4@SiO_2-Ag nanospheres which were prepared under optimum conditions (3 h) were chosen as a typical agent to plot the bacterial inhibition growth curves. Fig. 5 shows the antibacterial effect of the Fe_3O_4@SiO_2-Ag nanospheres against *Escherichia coli* and *Staphylococcus aureus* after culturing for 1 to 10 h. In comparison to the blank control groups, the growth rate of the *Escherichia coli* was clearly inhibited by using this nano-antibacterial agent (Fig. 5a). Even at a low concentration of nano-antibacterial agent (5 μg mL^{-1}), the bacteria were critically retarded. In this process, the higher the concentration, the better the antibacterial effects. Observably, the minimum inhibition concentration (MIC) of the Fe_3O_4@SiO_2-Ag nanospheres was just 20 μg mL^{-1}, which was smaller than the previously reported Ag-SiO_2, Ag-Fe_3O_4, and Ag-TiO_2.[48–50] Similarly, this nano-antibacterial agent also exhibited effective antibacterial activities to the *Staphylococcus aureus* with the MIC for *Staphylococcus aureus* estimated to be 40 μg mL^{-1} (Fig. 5b). *Staphylococcus aureus* and *Escherichia coli* are Gram-positive and Gram-negative bacteria respectively. It was reported that the membrane of the Gram-positive bacteria was thicker than the Gram-negative bacteria, thus the former was more stable than the latter.[51] To this end, it was reasonable to find that the *Escherichia coli* was more sensitive to Fe_3O_4@SiO_2-Ag nanospheres than the *Staphylococcus aureus*, which also agreed well with the previous work.

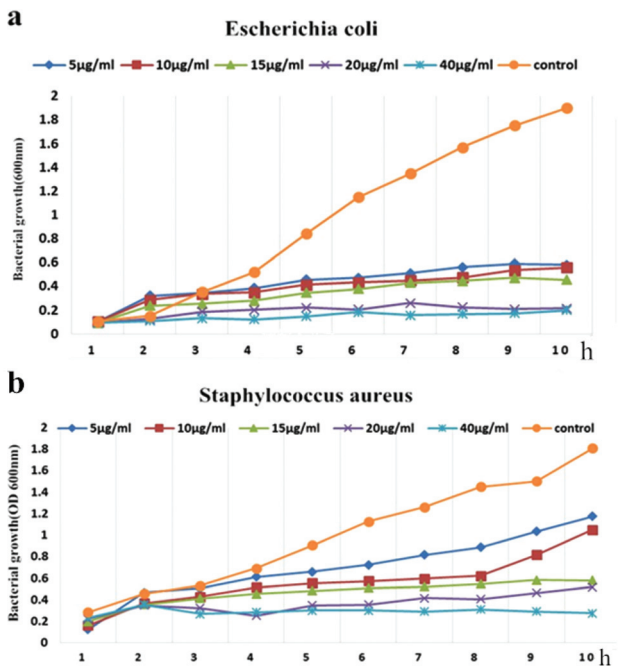

Fig. 5 Bacterial growth curves in Luria-Bertani (LB) media with Fe_3O_4@SiO_2-Ag nanospheres. Different concentrations of the nanospheres were used in cultures of *Escherichia coli* (a) and *Staphylococcus aureus* (b).

To further investigate the antibacterial activities of the Fe_3O_4@SiO_2-Ag nanospheres, a live/dead bacterial cell fluorescence stain assay was used to study the state of the bacterial cell before and after treatment with the antibacterial agent. In this work, after the bacterial cells were incubated with Fe_3O_4@SiO_2-Ag nanospheres for 12 h, a blue fluorescent dye was employed to stain the live cells. Fig. 6a shows the fluorescence image of the *Escherichia coli* without treatment with the nano-antibacterial agent. The strong blue fluorescence points in the image clearly indicate the living bacterial cells. However, after incubation, almost no fluorescence was observed (Fig. 6b). These results clearly indicate that the *Escherichia coli* cells were majorly inhibited in the presence of the nano-antibacterial agent. Moreover, similar results were also obtained for the *Staphylococcus aureus* (Fig. 6c and d), which further demonstrates that the as-prepared Fe_3O_4@SiO_2-Ag nanospheres showed unique effective antibacterial activities and these analyses agreed well with the observation from the antibacterial assays.

2.3 Cytotoxicity and uptake of the Fe_3O_4@SiO_2-Ag nanospheres to cancer cell

The Fe_3O_4@SiO_2-Ag nanospheres also exhibited relative cytotoxicity towards cancer cells. Hepatocellular carcinoma is the

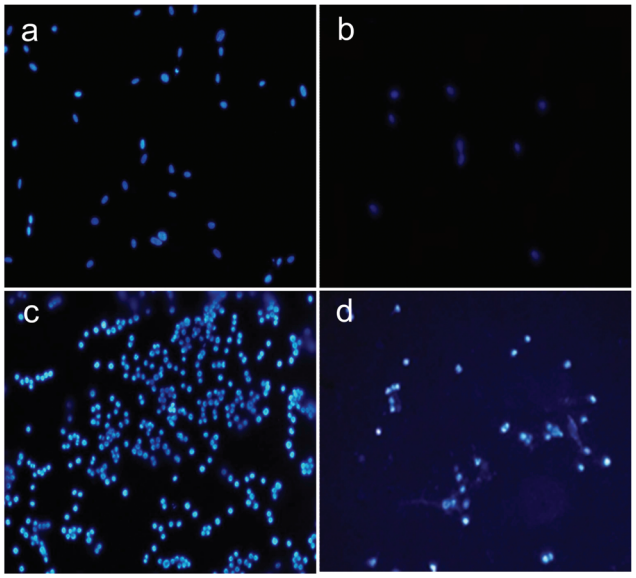

Fig. 6 Fluoresecnce images of the antibacterial activities of the Fe_3O_4@SiO_2-Ag nanospheres against *Escherichia coli* (a and b) and *Staphylococcus aureus* (c and d).

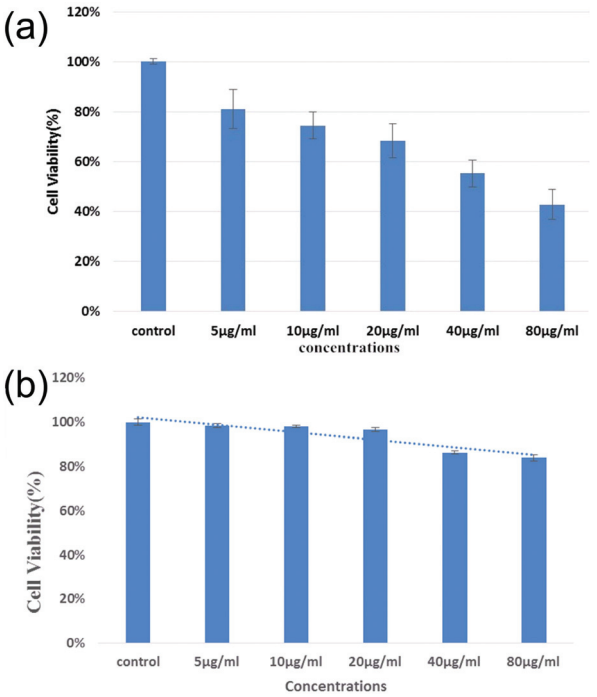

Fig. 7 *In vitro* cytotoxicity of Fe_3O_4@SiO_2-Ag nanospheres against HepG2 cells (a) and HUVEC cells (b) after incubation at 37 °C for 24 h.

fifth most-common cancer in the world. HepG2 is a perpetual cell line consisting of human liver carcinoma cells, thus they were chosen for testing the *in vitro* cytotoxicity of the as-prepared Fe_3O_4@SiO_2-Ag nanospheres. Firstly, the HepG2 cells were incubated with these nanospheres at 37 °C for 24 h. Then the *in vitro* cytotoxicity was measured using the Cell Counting Kit-8(CCK-8) assay. Here, the influence of the Fe_3O_4@SiO_2-Ag nanosphere concentration was also investigated in the range of 0–80 μg mL^{-1} (Fig. 7a). It was found that the Fe_3O_4@SiO_2-Ag nanospheres showed a unique effect on cytotoxicity against the HepG2 cells. Only 80% of cells were viable when a low concentration of these nanospheres (5 μg mL^{-1}) was introduced into the system. With an increase of nanosphere concentration, the cell viability decreased and it reduced to 44% when the concentration reached 80 μg mL^{-1}. Based on the above analysis, it could be concluded that the Fe_3O_4@SiO_2-Ag nanospheres were toxic to the cancer cells which enables them to be potentially applied as treating agents for cancer.

Safety is the main concern in the application of a nano-agent for clinical therapeutics, thus the cytotoxicity of the Fe_3O_4@SiO_2-Ag nanospheres to normal cells was investigated. In this work, the *in vitro* biocompatibility of the nanoparticles to HUVEC cells (Human Umbilical Vein Endothelial Cells) was tested by using the CCK-8 assay. As shown in Fig. 7b, the antibacterial materials did not present significant cytotoxicity against the HUVEC cells and the cell viability was maintained at 80% when the concentration of the nanospheres was increased to as high as 80 μg mL^{-1}. This indicates that the Fe_3O_4@SiO_2-Ag nanospheres showed good cytocompatibility with human normal cells.

The cellular uptake was studied to further investigate the action mechanism of the Fe_3O_4@SiO_2-Ag nanospheres to cancer cells. Here, Prussian blue staining was employed to evaluate the cellular uptake of the Fe_3O_4@SiO_2-Ag nanospheres in HepG-2 cells. Firstly, the HepG-2 cells were incubated with different concentrations of Fe_3O_4@SiO_2-Ag nanospheres for 20 h. Then, they were fixed for 30 min by using 4% paraformaldehyde. After treating them with Perls' reagent, the results were finally obtained using light microscopy. Fig. 8 shows the images of the Prussian blue stained cells with and without incubation with the Fe_3O_4@SiO_2-Ag nanospheres. Because of the monodispersity characteristic, these small Fe_3O_4@SiO_2-Ag nanospheres could insert into the cells very easily. Fig. 8b shows the image obtained by treating the cells with 10 μg mL^{-1} nanospheres. In comparison to the blank experiment, blue areas were clearly observed which indicates that the Fe_3O_4@SiO_2-Ag nanospheres were successfully uptaken by the HepG-2 cells. With increasing concentration, the uptake ratio increased (Fig. 8c and d). To this end, the high cellular uptake must be another reason for their excellent cytotoxicity. Moreover, these Fe_3O_4@SiO_2-Ag nanospheres were magnetic and they could target the disease area under application of a magnetic field. Since these nanospheres were bio-compatible to human normal cells, they could be used as a magnetic targeting therapeutic nano-agent for cancer cells without any terrible by-damage to the normal cells. To this end, the further investigation of these composite nanoparticles in cancer treatment was attractive.

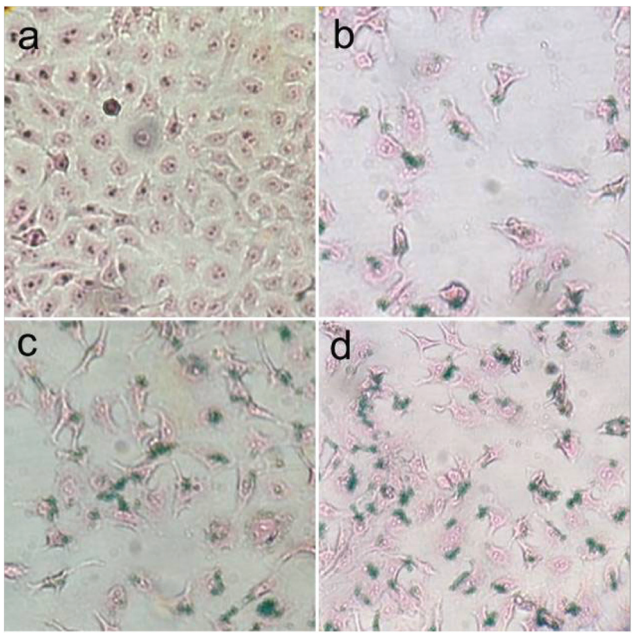

Fig. 8 Cellular uptake of Fe_3O_4@SiO_2-Ag nanospheres (a) 0, (b) 10, (c) 20, and (d) 40 μg mL^{-1} in HT29 cells evaluated by Prussian blue staining.

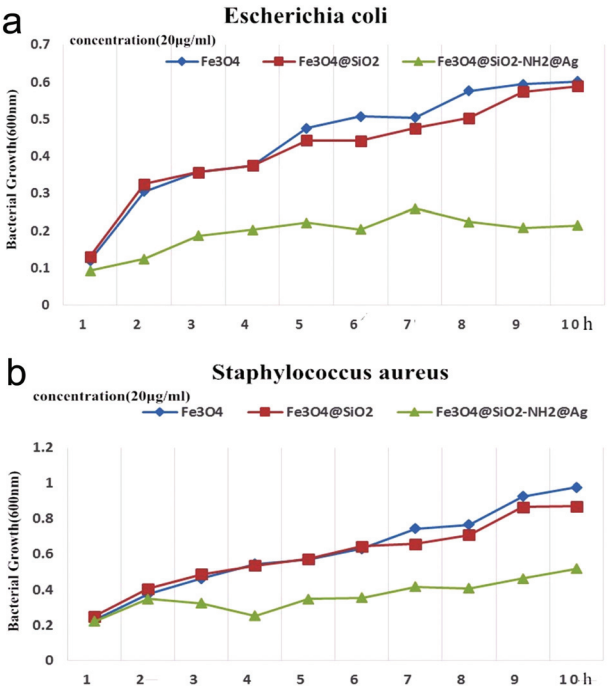

Fig. 9 Bacterial growth curves in LB media with Fe_3O_4, Fe_3O_4@SiO_2 and Fe_3O_4@SiO_2-Ag nanospheres. The concentration of the nanospheres was kept at 20 μg mL^{-1} in cultures of *Escherichia coli* (a) and *Staphylococcus aureus* (b).

2.4 The antibacterial mechanism of Fe_3O_4@SiO_2-Ag nanospheres

To further investigate the antibacterial mechanism, bacterial inhibition growth curves of the Fe_3O_4, Fe_3O_4@SiO_2 and Fe_3O_4@SiO_2-Ag nanospheres were obtained. Under the same dosage, Fe_3O_4 and Fe_3O_4@SiO_2 nanospheres could not inhibit the growth of both strains of bacteria, while the Fe_3O_4@SiO_2-Ag nanospheres showed significant inhibition of proliferation of the bacterial cells (Fig. 9). This result indicates that the antibacterial activity of the Fe_3O_4@SiO_2-Ag nanospheres comes from the Ag component immobilized on the surface of the Fe_3O_4@SiO_2 nanospheres.

On the basis of the above analysis and the results in the literature, the antibacterial activities of the Fe_3O_4@SiO_2-Ag nanospheres were ascribed to the following reasons: firstly, the antibacterial activity of the nanospheres was inherited from the Ag nanocrystals. Since these stable Ag nanodots were supported on the surface of the SiO_2 shell, they can exhibit an enhanced antibacterial activity by reacting with more sulfur-containing proteins in bacterial cells. Secondly, the Ag ions can be released from the nanocrystals and de-activate the microorganism cells. The average size of the Ag nanoparticles was only 3–5 nm in our product, thus the Ag ions might be released quicker than larger Ag nanoparticles. These released Ag ions would further cause structural changes to the cells and lead to their death. Thirdly, because of the small size of the uniform Fe_3O_4@SiO_2-Ag nanospheres, these particles could be uptaken by the cells very easily. More nanospheres could penetrate the cell membrane and directly kill the bacteria inside the cell membrane. Therefore, these Fe_3O_4@SiO_2-Ag nanospheres presented excellent antibacterial activities.

It was reported that the release behavior of the Ag ions from the Ag nanoparticles was pH dependent and more silver ions would be released in an acidic environment in comparison to a neutral buffer.[36] Moreover, the previous literature indicated that the pH of tumor cells is slightly more acidic than normal cells.[52] Therefore, more Ag ions would be released from the Ag nanoparticles in tumor cells than in human normal cells. To this end, the Fe_3O_4@SiO_2-Ag nanospheres exhibited higher cytotoxicity in HepG-2 cells than in HUVEC cells.

3. Experimental section

3.1 Preparation of the Fe_3O_4@SiO_2-Ag nanospheres

All chemicals were of analytical grade and used without further purification. First, the monodispersed Fe_3O_4 nanospheres which were prepared according to the previously reported method[42] were dispersed in an ethanol–H_2O–ammonia solution with a volume ratio of 30/3/1 under sonication. After half an hour, a certain amount of tetraethyl orthosilicate (TEOS) in ethanol (0.1/1 v/v) was added into the above system. 20 min later, 3-aminopropyltriethoxysilane (APTES) was dropped into the solution to graft $-NH_2$. After a further 30 min reaction under ultrasonication, the obtained Fe_3O_4@SiO_2-NH_2 nanospheres were collected by magnetic separation, washed with ethanol twice and then dispersed in ethanol. To immobilize the Ag nanoparticles onto the

Fe_3O_4@SiO_2-NH_2 nanospheres, the $[Ag(NH_3)_2]^+$ was firstly prepared by dissolving $AgNO_3$ in ammonia and then added into ethanol suspended Fe_3O_4@SiO_2-NH_2 nanospheres. Under sonication for 1 h, poly(vinylpyrrolidone) (PVP) (0.025 g mL^{-1}) was added into the system. The reaction was further conducted for 3 h and the final products were separated and rinsed with ethanol and water 3 times. After drying the particles in a vacuum oven for 12 h, the Fe_3O_4@SiO_2-Ag nanospheres were obtained.

3.2 Antibacterial assays

For the antibacterial activity assays, two bacterial species, *Escherichia coli* (Gram-negative bacteria) and *Staphylococcus aureus* (Gram-positive bacteria), were used in the experiments. Bacterial suspensions were prepared by taking a single colony from a stock bacterial culture with a loop and inoculating 5 mL of sterile nutrient broth medium, which was then incubated in a shaking incubator (37 °C at 200 rpm) for 12 h. Later, 30 mL bacterial suspensions were inoculated in 3 mL of liquid nutrient broth medium supplemented with different concentrations of the Fe_3O_4@SiO_2-Ag nanospheres. The suspensions were shaken using a shaker at 200 rpm at 37 °C, and their bacterial survival was determined by measuring the optical density (O.D.) of the nutrient broth in both media at a wavelength of 600 nm. The absorbance was sequentially checked from time 0 to 10 h at intervals of 1 h. To further examine the antibacterial properties, the bacteria were stained with the live/dead Bacterial Viability Kit following the standard protocol (GENMED). Briefly, 3 μL of the fluorescently dyed mixture was added into each milliliter of the bacterial suspensions. Then, the samples were thoroughly mixed and incubated at room temperature in the dark for 15 minutes. To observe the image with a fluorescence microscope, 5 μL of the stained bacterial suspension was added to a slide with a square cover slip. For comparison, the antibacterial assays of the Fe_3O_4, Fe_3O_4@SiO_2, and Fe_3O_4@SiO_2-Ag nanospheres were performed under the same process while keeping the concentration of the nanospheres at 20 μg mL^{-1}.

3.3 Cell culture and *in vitro* cell viability evaluation

HepG2 cells were purchased from the American Type Culture Collection and were cultured in Dulbecco's modified Eagle's medium (GIBCO,USA) supplemented with 10% fetal bovine serum (GIBCO,USA), 2 mM L-glutamine, 100 μg mL^{-1} streptomycin and 100 U mL^{-1} penicillin. The cells were cultured in a 37 °C humidified atmosphere with 5% CO_2. The *in vitro* cytotoxicity of the Fe_3O_4@SiO_2-Ag nanospheres against HepG-2 cells was tested using the Cell Counting Kit-8 assay. The cells were seeded in 96-well plates with a density of 1×10^4 cells per well in 100μL of DMEM supplemented with 10% FBS cultured in a humidified atmosphere of 5% CO_2 at 37 °C for 24 h. Then, the HepG-2 cells were incubated in the growth medium containing different concentrations (5, 10, 20, 40 and 80 μg mL^{-1}) of the Fe_3O_4@SiO_2-Ag nanospheres for another 24 h. Meanwhile, wells containing the cell medium only were prepared for the untreated controls. Then, 10 μL of CCK-8 dye was added to each well and the plates were incubated for another 2 h at 37 °C. The absorbance was measured using single wavelength spectrophotometry at 450 nm using a microplate reader. The relative cell viability was determined by comparing the absorbance at 450 nm with the control wells that contained the cell culture medium only.

3.4 Cellular uptake

The cellular uptake of the Fe_3O_4@SiO_2-Ag nanospheres was evaluated in HepG-2 cells using Prussian blue staining. HepG-2 cells were seeded in a 96-well plate in DMEM containing 10% FBS. After 12 h incubation, the medium was replaced with serum-free DMEM containing different concentrations (0, 10, 20, and 40 μg mL^{-1}) of the Fe_3O_4@SiO_2-Ag nanospheres and incubated for another 20 h. For the Prussian blue staining, the cells were fixed for 30 min by using 4% paraformaldehyde. After washing with PBS, the cells were incubated with Perls' reagent (4% potassium ferrocyanide and 6% HCl) for 30 min, followed by a neutral red counterstain. Then the cells were observed using a light microscope.

3.5 Characterization

X-ray powder diffraction patterns (XRD) of the products were obtained using a Bruker D8 Advance diffractometer equipped with graphite monochromatized Cu Kα radiation (λ = 1.5406 Å). Transmission electron microscopy (TEM) photographs were taken using a high-resolution transmission electron microscope (Tecnai Model JEOL-2010) at an accelerating voltage of 200 kV. The field emission scanning electron microscopy (FE-SEM) images were taken using a JEOL JSM-6700F SEM. X-ray photoelectron spectra were measured using an ESCALAB 250.

4. Conclusions

In summary, we present an environmentally friendly method to synthesize monodisperse Fe_3O_4@SiO_2-Ag nanospheres under ultrasonication. No toxic reagent was used in the synthesis and the final Ag nanocrystals were uniformly immobilized onto the periphery of Fe_3O_4@SiO_2-NH_2 nanospheres. The antibacterial assay indicated that the Fe_3O_4@SiO_2-Ag nanospheres exhibited excellent antibacterial activities against *Staphylococcus aureus* and *Escherichia coli*, in which the MIC were 40 μg mL^{-1} and 20 μg mL^{-1}, respectively. Moreover, these nanospheres were demonstrated to be cytotoxic towards HepG2 while being compatible with human normal cells. Due to their magnetic characteristics, they could be applied in targeting treatment. The average size of these nanospheres was about 200 nm, thus they could easily be uptaken by the HepG2 cells. To this end, this kind of nanospheres presented high antibacterial performance since they could destroy the bacterial cells both outside and inside the cell membrane.

Acknowledgements

We acknowledge financial support from the National Natural Science Foundation of China (grant no. 21205026), HKRGC-GRF (201412), and the University Grants Committee of Hong Kong SAR (AoE/P-03/08).

Notes and references

1 S. Q. Li and N. P. Shah, *Food Chem.*, 2014, **165**, 262–270.
2 M. Rai, A. Yadav and A. Gade, *Biotechnol. Adv.*, 2009, **27**, 76–83.
3 I. Kouidmi, R. C. Levesque and C. Paradis-Bleau, *Mol. Microbiol.*, 2014, **94**, 242–253.
4 C. Marambio-Jones and E. M. V. Hoek, *J. Nanopart. Res.*, 2010, **12**, 1531–1551.
5 Q. L. Li, S. Mahendra, D. Y. Lyon, L. Brunet, M. V. Liga, D. Li and P. J. J. Alvarez, *Water Res.*, 2008, **42**, 4591–4602.
6 O. L. Galkina, A. Sycheva, A. Blagodatskiy, G. Kaptay, V. L. Katanaev, G. A. Seisenbaeva, V. G. Kessler and A. V. Agafonov, *Surf. Coat. Technol.*, 2014, **253**, 171–179.
7 W. B. Hu, C. Peng, W. J. Luo, M. Lv, X. M. Li, D. Li, Q. Huang and C. H. Fan, *ACS Nano*, 2010, **4**, 4317–4323.
8 J. Lee, S. Mahendra and P. J. J. Alvarez, *ACS Nano*, 2010, **4**, 3580–3590.
9 O. Akhavan, M. Abdolahad, Y. Abdi and S. Mohajerzadeh, *J. Mater. Chem.*, 2011, **21**, 387–393.
10 J. R. Morones, J. L. Elechiguerra, A. Camacho, K. Holt, J. B. Kouri, J. T. Ramirez and M. J. Yacaman, *Nanotechnology*, 2005, **16**, 2346–2353.
11 R. Xiong, C. H. Lu, Y. R. Wang, Z. H. Zhou and X. X. Zhang, *J. Mater. Chem. A*, 2013, **1**, 14910–14918.
12 I. Sondi and B. Salopek-Sondi, *J. Colloid Interface Sci.*, 2004, **275**, 177–182.
13 T. M. Benn and P. Westerhoff, *Environ. Sci. Technol.*, 2008, **42**, 4133–4139.
14 M. Nocchetti, A. Donnadio, V. Ambrogi, P. Andreani, M. Bastianini, D. Pietrella and L. Latterini, *J. Mater. Chem. B*, 2013, **1**, 2383–2393.
15 H. Y. Lee, H. K. Park, Y. M. Lee, K. Kim and S. B. Park, *Chem. Commun.*, 2007, 2959–2961.
16 K. Chaloupka, Y. Malam and A. M. Seifalian, *Trends Biotechnol.*, 2010, **28**, 580–588.
17 Q. L. Feng, J. Wu, G. Q. Chen, F. Z. Cui, T. N. Kim and J. O. Kim, *J. Biomed. Mater. Res.*, 2000, **52**, 662–668.
18 Y. Matsumura, K. Yoshikata, S. Kunisaki and T. Tsuchido, *Appl. Environ. Microbiol.*, 2003, **69**, 4278–4281.
19 Z. M. Xiu, Q. B. Zhang, H. L. Puppala, V. L. Colvin and P. J. J. Alvarez, *Nano Lett.*, 2012, **12**, 4271–4275.
20 R. Ma, C. Levard, S. M. Marinakos, Y. Cheng, J. Liu, F. M. Michel, G. E. Brown and G. V. Lowry, *Environ. Sci. Technol.*, 2012, **46**, 752–759.
21 G. X. Gu, J. X. Xu, Y. F. Wu, M. Chen and L. M. Wu, *J. Colloid Interface Sci.*, 2011, **359**, 327–333.
22 Z. W. Deng, H. B. Zhu, B. Peng, H. Chen, Y. F. Sun, X. D. Gang, P. J. Jin and J. L. Wang, *ACS Appl. Mater. Interfaces*, 2012, **4**, 5625–5632.
23 B. Chudasama, A. K. Vala, N. Andhariya, R. V. Upadhyay and R. V. Mehta, *Nano Res.*, 2009, **2**, 955–965.
24 S. Poyraz, I. Cerkez, T. S. Huang, Z. Liu, L. T. Kang, J. J. Luo and X. Y. Zhang, *ACS Appl. Mater. Interfaces*, 2014, **26**, 20025–20034.
25 P. C. Ma, B. Z. Tang and J. K. Kim, *Carbon*, 2008, **46**, 1497–1505.
26 K. Y. Chun, Y. Oh, J. Rho, J. H. Ahn, Y. J. Kim, H. R. Choi and S. Baik, *Nat. Nanotechnol.*, 2010, **5**, 853–857.
27 R. Pasricha, S. Gupta and A. K. Srivastava, *Small*, 2009, **5**, 2253–2259.
28 C. P. Chen, P. Gunawan, X. W. Lou and R. Xu, *Adv. Funct. Mater.*, 2012, **22**, 780–787.
29 M. Liong, B. France, K. A. Bradley and J. I. Zink, *Adv. Mater.*, 2009, **21**, 1684–1689.
30 J. Z. Ma, J. T. Zhang, Z. G. Xiong, Y. Yong and X. S. Zhao, *J. Mater. Chem.*, 2011, **21**, 3350–3352.
31 A. Gupat, M. Maynes and S. Silver, *Appl. Environ. Microbiol.*, 1998, **64**, 5042–5045.
32 X. Wang, Y. Dai, J. L. Zou, L. Y. Meng, S. Ishikawa, S. Li, M. Abuobeidah and H. G. Fu, *RSC Adv.*, 2013, **3**, 11751–11758.
33 M. M. Khin, A. S. Nair, V. J. Babu, R. Murugan and S. Ramakrishna, *Energy Environ. Sci.*, 2012, **5**, 8075–8109.
34 A. Pratsinis, P. Hervella, J. C. Leroux, S. E. Pratsinis and G. A. Sotiriou, *Small*, 2013, **9**, 2576–2584.
35 X. L. Zhang, H. Y. Niu, J. P. Yan and Y. Q. Cai, *Colloids Surf., A*, 2011, **375**, 186–192.
36 S. Mukherjee, D. Chowdhury, R. Kotcherlakota, S. Patra, B. Vinothkumar, M. P. Bhadra, B. Sreedhar and C. R. Patra, *Theranostics*, 2014, **4**, 316–335.
37 Y. Cong, T. Xia, M. Zou, Z. N. Li, B. Peng, D. Z. Guo and Z. W. Deng, *J. Mater. Chem. B*, 2014, **2**, 3450–3461.
38 P. Dalla, J. Tucek, D. Jancik, M. Kolar, A. Panacek and R. Zboril, *Adv. Funct. Mater.*, 2010, **20**, 2347–2354.
39 H. Wang, J. Shen, G. X. Gao, Z. Gai, K. L. Hong, P. R. Debata, P. Banerjee and S. Q. Zhou, *J. Mater. Chem. B*, 2013, **1**, 6225–6234.
40 H. H. Park, S. J. Park, G. P. Ko and K. Woo, *J. Mater. Chem. B*, 2013, **1**, 2701–2709.
41 L. Zhang, Q. Luo, F. Zhang, D. M. Zhang, Y. S. Wang, Y. L. Sun, W. F. Dong, J. Q. Liu, Q. S. Huo and H. B. Sun, *J. Mater. Chem.*, 2012, **22**, 23741–23744.
42 Y. J. Chen, N. Gao and J. Jiang, *Small*, 2013, **9**, 3242–3246.
43 S. H. Xuan, Y. X. J. Wang, J. C. Yu and K. C.-F. Leung, *Chem. Mater.*, 2009, **21**, 5079–5087.
44 K. S. Suslick, *Science*, 1990, **247**, 1439–1445.
45 S. H. Xuan, Y.-X. J. Wang, J. C. Yu and K. C.-F. Leung, *Langmuir*, 2009, **25**, 11835–11843.
46 H. P. Klug and L. E. Alexander, *X-ray Diffraction Procedures for Polycrystalline and Amorphous Materials*, Wiley, New York, 1962, pp. 491–538.

47 D. Lee, R. E. Cohen and M. F. Rubner, *Langmuir*, 2005, **21**, 9651–9659.
48 S. Egger, R. P. Lehmann, M. J. Height, M. J. Loessner and M. Schuppler, *Appl. Environ. Microbiol.*, 2009, **75**, 2973–2976.
49 P. Gong, H. Li, X. He, K. Wang, J. Hu, W. Tan, S. Zhang and X. Yang, *Nanotechnology*, 2007, **18**, 285604.
50 N. Nino-Martinez, G. A. Martinez-Castanon, A. Aragon-Pina, F. Martinez-Gutierrez, J. R. Martinez-Mendoza and F. Ruiz, *Nanotechnology*, 2008, **19**, 065711.
51 J. Njagi, M. M. Chernov, J. C. Leiter and S. Andreescu, *Anal. Chem.*, 2010, **82**, 989–996.
52 I. F. Tannock and D. Rotin, *Cancer Res.*, 1989, **49**, 4373–4384.